Journal of Cerebral Blood Flow & Metabolism (2010) 30, 428–439

www.jcbfm.com

Changes in cerebral arterial, tissue and venous oxygenation with evoked neural stimulation: implications for hemoglobin-based functional neuroimaging

Alberto L Vazquez[1], Mitsuhiro Fukuda[1], Michelle L Tasker[1], Kazuto Masamoto[2] and Seong-Gi Kim[1,3]

[1]*Department of Radiology, University of Pittsburgh, Pittsburgh, Pennsylvania, USA;* [2]*Molecular Imaging Center, National Institute of Radiological Sciences, Chiba, Japan;* [3]*Department of Neurobiology, University of Pittsburgh, Pittsburgh, Pennsylvania, USA*

Little is known regarding the changes in blood oxygen tension (P_{O2}) with changes in brain function. This work aimed to measure the blood P_{O2} in surface arteries and veins as well as tissue with evoked somato-sensory stimulation in the anesthetized rat. Electrical stimulation of the forepaw induced average increases in blood flow of 44% as well as increases in the tissue P_{O2} of 28%. More importantly, increases in P_{O2} throughout pial arteries (resting diameters = 59 to 129 μm) and pial veins (resting diameters = 62 to 361 μm) were observed. The largest increases in vascular P_{O2} were observed in the small veins (from 33 to 40 mm Hg) and small arteries (from 78 to 88 mm Hg). The changes in oxygen saturation (S_{O2}) were calculated and the largest increases were observed in small veins (Δ = + 11%) while its increase in small arteries was small (Δ = + 4%). The average diameter of arterial vessels was observed to increase by 4 to 6% while that of veins was not observed to change with evoked stimulation. These findings show that the increases in arterial P_{O2} contribute to the hyper-oxygenation of tissue and, mostly likely, also to the signal changes in hemoglobin-based functional imaging methods (e.g. BOLD fMRI).
Journal of Cerebral Blood Flow & Metabolism (2010) **30,** 428–439; doi:10.1038/jcbfm.2009.213; published online 21 October 2009

Keywords: BOLD fMRI; CBF; CMRO2; Oxygen; Hemoglobin; OIS

Introduction

It is well known that the brain requires oxygen to maintain its normal baseline function; however, the role of oxygen to satisfy changes in neural activity is less clear. A thorough understanding of the dynamics of oxygen supply and consumption is important not only because neuronal vitality relies on oxygen availability, but also because a large number of functional imaging techniques (e.g. functional magnetic resonance imaging (fMRI) and optical imaging of intrinsic signal (OIS)) rely on the concomitant changes in blood oxygenation to image brain function. Physiologically, changes in cerebral blood flow (CBF) and cerebral oxygen consumption (CMR_{O2}) have been measured with evoked neural stimulation (Kwong *et al*, 1992; Kim, 1995; Kim *et al*, 1999; Davis *et al*, 1998; Mayhew, *et al.*, 2000; Boas *et al*, 2003; Shulman *et al*, 2001). Both of these processes modulate the oxygen concentration in both vessels and tissue. In the vessels, increases in blood flow decrease the longitudinal gradient of oxygen along the vascular tree, effectively increasing the venous and tissue oxygenation (Davis *et al*, 1998; Kim *et al*, 1999; Berwick *et al*, 2005). In the tissue, increases in oxygen consumption decrease the tissue and venous oxygen concentration (Fukuda *et al*, 2006). Under normal conditions, both of these processes take place and the overall tissue oxygenation also increases due to an enhanced transport of oxygen from vessel to tissue at the capillary level (i.e. a larger transmural oxygen gradient). One might imagine that the functional role of blood flow is to maintain a constant tissue oxygen tension, however, the increase in tissue oxygenation has been reported to exceed the tissue oxygen consumption by more than a factor of two (Weiss *et al*, 1983; Vazquez *et al*, 2008). As a result, an in-depth understanding of the delivery of oxygen, including the more general mechanism(s)

Correspondence: Dr AL Vazquez, Department of Radiology, University of Pittsburgh, 3025 E Carson St, McGowan Center BIRC Rm 159, Pittsburgh, PA, 15203, USA.
E-mail: alv15@pitt.edu
Received 5 March 2009; revised 20 August 2009; accepted 15 September 2009; published online 21 October 2009

driving the changes in oxygen transport to neurally active brain tissue, has remained elusive. Many functional imaging methods rely on these changes in blood oxygenation to image and also quantify brain function. Quantitative fMRI studies have relied on measurements of evoked physiological changes like CBF and also on the normalization of BOLD signal changes which have been collectively used to calculate CMR_{O2}. However, the quantification of functional changes in blood oxygenation suffers from assumptions of the oxygen transport properties (e.g. no functional changes in arterial oxygenation), many of which have not been verified.

Optical methods have long been used for oximetry where the oxygen saturation of blood hemoglobin is calculated by measuring its absorption of light at different wavelengths (Severinghaus, 1993; Boas *et al*, 2001). However, quantification from spatially specific locations using optical imaging suffers from several setbacks, including the lack of depth selectivity which results in unwanted signal contributions from beyond the cortical surface. This drawback has long been advantageously used in optical imaging studies to gain intra-cortical sensitivity from this largely surface-biased technique. As a result, less complex, single-wavelength optical imaging experiments are commonly performed where the sensitivity to oxygen saturation is preserved though not readily quantifiable, similar to BOLD fMRI. To quantify the dynamics of oxygen transport from blood to tissue more selective techniques are desired. Alternatively, Clark-type oxygen sensors have been classically used to measure oxygen tension in tissue and blood vessels (Ances *et al*, 2001; Masamoto *et al*, 2003; Thompson *et al*, 2003; Vovenko, 1999; Tsai *et al*, 2003). Although they only record a point measurement, their spatial resolution typically span tens to a few hundred microns. In addition, their temporal resolution has been shown to be sufficient to see transient decreases and increases in tissue oxygen tension.

In a previous report by our group, the dynamic properties of oxygen delivery and consumption were investigated using a model of the transport of oxygen from blood to tissue along with CBF and tissue oxygen tension (P_{O2}) data (Vazquez *et al*, 2008). The changes in oxygen delivery to tissue were estimated to be about 2.7×larger than the tissue oxygen consumption. While this work explored much of the dynamics of oxygen transport to tissue, largely unanswered questions that remain include: (1) How does the longitudinal gradient from arteries to veins change with brain function? In particular, where do the changes in oxygenation take place, to what extent, and, quantitatively, by how much? (2) How do the changes in regional cerebral arterial oxygenation, if any, contribute to the delivery of oxygen in tissue? (3) How are these changes represented in different imaging/measurement methods? The primary objective of this work was to measure the changes in cerebral oxygenation of surface arteries, arterioles, venules, veins and tissue produced by oxygen delivery and oxygen consumption in order to investigate these questions. Simultaneous measurements of the arterial, tissue and venous P_{O2} were obtained using Clark-type oxygen sensors during evoked stimulation of the rat somatosensory cortex and CBF was measured using laser Doppler flowmetry.

Materials and methods

Animal Preparation

A total of nine male Sprague-Dawley rats (330 to 480 g) were used in this work following an experimental protocol approved by the University of Pittsburgh Institutional Animal Care and Use Committee. The animals were initially anesthetized using isoflurane (5% for induction, 2% for surgery), nitrous oxide (50 to 65%) and oxygen (35 to 50%) for intubation and placement of catheters in the femoral artery and femoral vein. The respiration rate and volume were controlled using a ventilator (TOPO, Kent Scientific, Torrington, CT). After intubation, the animals were placed in a stereotaxic frame (Narishige, Tokyo, Japan) and the skull was exposed over the somato-sensory area. A well was made using dental acrylic surrounding an area 5 mm × 7 mm on the left side of the skull, centered 3.5 mm lateral and 1.5 mm rostral from Bregma (Hall *et al*, 1974). The skull in this area was then removed using a dental drill. The dura matter was resected and the CSF fluid was released around the fourth ventricle area to minimize herniation. The well and the CSF release areas were then filled with 1.0% agarose gel at body temperature. Two needle electrodes were placed in the right forepaw between digits 2 and 4 for electrical stimulation. The anesthesia and breathing mixture were then changed to isoflurane (1.5%), oxygen (~10%) and air (~90%). Rectal temperature was maintained at 37.0 °C throughout with a DC temperature control module (40-90-8C, FHC Inc., Bowdoinham, ME). Arterial blood sampling was periodically performed to measure systemic arterial blood oxygen tension (P_{aO2}), arterial carbon dioxide tension (P_{aCO2}), pH, hemoglobin concentration ([Hb]) and hematocrit (Hct) using a blood gas analyzer (Stat Profile, Nova Medical Corp., Waltham, MA). The arterial blood pressure, respiration rate, heart rate, rectal temperature, end-tidal CO_2 tension and isoflurane level were monitored and recorded using a polygraph data acquisition software (Acknowledge, Biopac Systems Inc., Goleta, CA).

Experimental Design

The general experimental procedure was similar to our previous study (Masamoto *et al*, 2008). Initially, a short stimulation experiment was performed to locate the activation area using optical imaging of intrinsic signal (OIS at 620 nm with bandwidth of 10 nm). At this wavelength, deoxygenated hemoglobin absorbs about 4×more light than oxygenated hemoglobin (Horecker, 1943). Then, Clark-type oxygen sensors (Unisense,

Aarhaus, Denmark) and a needle-type laser Doppler probe (diameter of 450 μm and operating wavelength of 780 nm; Perimed, Stockholm,Sweden) were positioned over the targeted locations to simultaneously measure P_{O2} and CBF. OIS was also simultaneously recorded in most experiments. The P_{O2} in tissue and blood were measured using sensors with tip diameters of 30 and 4 μm, respectively. The spatial sensitivity of the oxygen sensors spans at most $10\times$ their tip diameter (Fatt, 1976), and these were selected to sample a relatively large volume of tissue (30 μm probe) and restrict the vascular P_{O2} measurements to the vascular space (4 μm probes) since the vessels sampled were at least 40 μm in diameter. The spatial sensitivity of the LDF probe used spans a volume of 1 mm^3. The oxygen sensors were calibrated before and after each experiment with 0%, 21% and 100% oxygen in saline solution at 37 °C.

Pre-mapping and Probes Placement

To map the activation area, OIS images were obtained during 4 secs of electrical forepaw stimulation delivered using a pulse generator and isolator (Master 8 and ISO-Flex, A.M.P.I., Jerusalem, Israel). The stimulus consisted of 48 pulses with duration of 1.0 ms, amplitude of 1.6 mA and frequency of 12 Hz (4 secs) repeated every 16 secs for 165 secs. The OIS images were obtained using an analog CCD camera mounted on a macroscope (Olympus MVX-10, Olympus Inc., Tokyo, Japan). Images were captured at 30 frames per second using a frame grabbing board and custom software with resolution of 640×480 pixels and field-of-view between 4.6×3.5 and 9.3×7.0 mm^2 depending on the magnification. A differential analysis was performed where the average image obtained 1 sec prior to stimulation onset in each trial was subtracted from each image in the trial; all trials were then averaged (a sample pre-mapping image series is presented in Figure 5A). The resulting data were used to calculate the centroid of the activation area based on the magnitude of the negative change in the reflected OIS signal (i.e. increase in absorption) observed 1 to 2 secs after stimulus onset.

To simultaneously record tissue and blood P_{O2} as well as CBF responses, three oxygen sensors and a LDF probe were carefully placed in close proximity over the activation area (see Figure 1). A Clark-type oxygen sensor was first placed in the tissue near the centroid of the active region at a depth of 300 μm. Often this sensor was placed lateral to both the targeted arterial and venous vessel locations to maintain accessibility. Another Clark-type sensor was then placed on the superior surface of a selected artery supplying blood to the active area. Preliminary testing of the spatial sensitivity of the probe for intra-luminal vs surface recordings determined that this placement is sensitive to the vessel oxygen tension, in agreement with similar studies (Vovenko, 1999; Sharan, *et al*, 2008). Three positions were sampled along the selected artery: one just prior to its intra-cortical penetrating point (referred to as small artery, SmArt or SA) and two upstream parent branches (referred to as medium and large artery, or MedArt and LarArt, or MA and LA, respectively). The location of the probe on the artery was verified visually and also by the relatively high P_{O2} reading. Then, another Clark-type oxygen tension probe was placed on the superior surface of a selected vein in close proximity to the selected artery and draining blood from within the activation area. Similarly, three positions were sampled along the selected vein: one just after its emerging intra-cortical location (referred to as small vein or SmVen or SV) and two downstream parent branches (referred to as medium and large vein, or MedVen and LarVen, or MV and LV, respectively). Lastly, the LDF was positioned such that it spanned the small artery, tissue and small vein areas as best as possible.

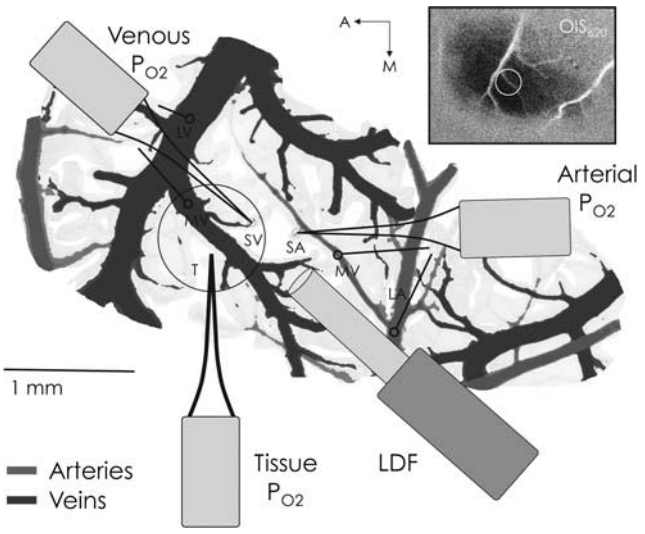

Figure 1 Sample diagram of the oxygen sensors (P_{O2}) and laser Doppler flowmeter (LDF) probe placement. The blood vessel pattern depicted in this figure was obtained by tracing an image of the surface vessels recorded from this subject. For each experiment in a subject, the arterial and venous P_{O2} probes were placed on a small pre-penetrating surface artery (SA or SmArt) and a small emerging surface vein (SV or SmVen), respectively, and also in their larger parent vessels; namely, medium artery (MA or MedArt) and medium vein (MV or MedVen), and large artery (LA or LarArt) and large vein (LV or LarVen). The other locations sampled are represented by open circles with lines leading to the appropriate probe that sampled that location. The inset shows the actual average OIS image from which the centroid of activity was calculated.

Measurements of the intra-luminal vessel diameters at the sampled locations were made from a surface image acquired at a wavelength of 570 nm, which is near equally sensitive to oxy- and deoxy-hemoglobin. The vascular distance between the sampled locations was also calculated.

Simultaneous P_{O2}, CBF and OIS measurements

Experiments were performed while simultaneous measurements of arterial P_{O2}, tissue P_{O2}, venous P_{O2} and LDF were recorded from their selected locations during 20 secs of electrical forepaw stimulation. The stimulus consisted of 60 pulses (1.0 ms in duration and amplitude of 1.6 mA) delivered at a frequency of 3 Hz every 80 secs for 650 secs. In all animals tested, the location of the tissue P_{O2} and LDF

probes was fixed after placement. In three animals, only the small artery and small vein locations were sampled. In all other animals, small, medium and large vessel locations were sampled in separate experiments and in pseudo-random order. The P_{O2} and LDF signals were recorded at 1 kHz using the polygraph recording software. In most studies (8 of 9), OIS was also recorded as described above (see Pre-mapping section).

Data Analysis

All the data were analyzed using Matlab (Natick, MA) and all the population data are reported as mean ± s.d., unless otherwise specified. After recording the LDF and P_{O2} data, the various trials within each experimental condition were averaged. The P_{O2} data were then converted to absolute P_{O2} using the calibration curves determined for each animal. The P_{O2} measurement lag was also corrected (measured independently to be 1.0, 0.6 and 0.6 secs to 90% of the final amplitude for the tissue, arterial and venous oxygen sensor used) by deconvolution with an exponential function. The resulting data were then low-pass filtered with a 5 Hz rectangular cut-off. The average oxygen saturation fraction time series were calculated for each sampled vessel location using the Hill equation with exponent of 2.73 and P50 of 38 mm Hg (Gray and Steadman 1964). This calculation assumes that the concentration of oxygen dissolved in plasma (measured by the P_{O2} probe) rapidly associates/dissociates with hemoglobin in red blood cells. Indeed, this process has been measured to be rapid, taking around tens of milliseconds under normal conditions (Popel, 1989; Gibson *et al*, 1955). The baseline P_{O2} and LDF values were calculated by averaging the data over 5 secs prior to stimulation onset. The activation values were calculated by the average of the data between 10 and 20 secs after stimulation onset. Student's *t*-tests were performed to test the significance of the increases in P_{O2} and LDF with stimulation. The significance of the oxygen tension gradient was determined by paired *t*-tests between the large artery location and all the other locations.

The optical imaging of intrinsic signal data (620 nm light) were analyzed as follows. A total of eight ROIs were outlined, one for each vessel location sampled, positioned on the blood vessel adjacent to the respective probe's sampling location (for a total of six ROIs), another centered on the penetration point of the tissue P_{O2} sensor spanning a diameter of 100 μm (excluding the probe), and another covering a 500 μm diameter region over the centroid location. A sample location of the vessel ROIs in one subject is presented in Figure 5B (bottom-right panel). In two OIS studies, the medium and large arteries and veins locations were not sampled by P_{O2}; nonetheless, the OIS ROIs were positioned on the parent branches of the vessels sampled. The temporal series from these ROIs were temporally averaged to a nominal resolution of 10 Hz and baseline normalized as done above for the P_{O2} and LDF data. Lastly, the changes in vessel diameter as a function of time were calculated for the large artery, medium artery, medium and large vein locations by placing a four-pixel width ROI perpendicular to the vessel direction. The image within the ROI was linearly interpolated and the intensity along the four-pixel direction was then summed in order to obtain projected intensity profiles. This yielded the intraluminal vessel profile and its full-width-at-half-minimum (FWHM) was measured. Assuming the vessel is cylindrical, the actual diameter corresponds to 15.5% over the FWHM value. This method is illustrated in Supplementary Figure S1 in the Supplementary Material.

Estimates of the onset time were obtained from the P_{O2} and OIS time series by measuring the time-to-20%-peak amplitude (t_{20}) and time-to-50%-dip amplitude (t_{50-dip}). Paired t-tests were performed to test for significance. The average temporal latencies between the different P_{O2} time series were investigated by generating scatter plots of the average P_{O2} time series.

Results

Baseline Measurements

The physiological parameters of all the animals tested were maintained within normal physiological levels. The mean arterial blood pressure (MABP) was measured to be, on average, 89 mm Hg at the femoral artery, and average blood gas measurements from the same location yielded a pH of 7.45, P_{CO2} of 37.6 mm Hg, P_{O2} of 133.3 mm Hg, [Hb] of 11.1 g/dL, and Hct of 33.3% (for further details see Supplementary Table S1).

Six vessel locations were targeted for oxygen tension measurements (P_{O2}) and their average intraluminal diameters vessels were: 128.9 μm (large artery), 84.0 μm (medium artery), 52.7 μm (small artery), 61.9 μm (small vein), 144.6 μm (medium vein) and 361.0 μm (large vein; see Table 1). The average vascular path between the sampled large and medium artery locations and the medium and small artery locations were measured to be 1914.5 ± 1683.2 μm and 783.1 ± 788.0 μm, respectively ($n = 6$). The average distance following the vascular tree between the sampled small and medium vein locations and the sampled medium and large vein locations were measured to be 548.1 ± 223.2 μm and 2645.8 ± 2681.0 μm, respectively ($n = 6$). The average distance between the sampled locations of the small artery and the small vein was 437.4 ± 319.5 μm, while the average distance between the sampled small artery and tissue and the sampled small vein and tissue was 969.2 ± 542.9 μm ($n = 9$). The average oxygen tensions and oxygen saturations at the sampled locations are reported in Table 1.

Stimulation-induced P_{o2} and CBF Responses

Forepaw stimulation for 20 secs induced significant changes in CBF and P_{O2} in all the locations measured (see Figure 2 and Table 1). On average, increases of 43.9% were observed in CBF over the last 10 secs of the stimulation period. Similarly, average increases

Table 1 Vessel diameter, resting and active P_{O2} values, and calculated resting and active S_{O2} values at the targeted sampled locations

Location	*Vessel Diameter (μm)*	*Resting P_{O2} (mm Hg)*	*Active P_{O2} (mm Hg)*	*P_{O2} Change (mm Hg)*	*Resting S_{O2} %*	*Active S_{O2} %*	*S_{O2} Change %*
Femoral artery ($n=9$)	N/A	133.3 ± 8.7	N/A	N/A	96.9 ± 0.6	N/A	N/A
Large Artery ($n=6$)	128.9 ± 36.3	88.1 ± 20.5	91.9 ± 18.5	3.8 ± 3.1	88.3 ± 9.9	89.8 ± 6.9	1.6 ± 3.1
Medium Artery ($n=6$)	84.0 ± 37.3	89.2 ± 29.7	94.1 ± 28.4	4.8 ± 2.8	86.8 ± 13.1	88.9 ± 10.6	2.1 ± 2.5
Small Artery ($n=9$)	52.7 ± 17.6	77.9 ± 24.9	88.4 ± 21.8	10.5 ± 5.9	81.6 ± 10.9	85.9 ± 10.6	4.3 ± 9.6
Tissue ($n=9$)	N/A	38.0 ± 15.1	48.5 ± 14.1	10.5 ± 4.4	N/A	N/A	N/A
Small Vein ($n=9$)	61.9 ± 15.5	33.3 ± 7.2	40.4 ± 8.0	7.1 ± 6.6	40.5 ± 14.5	51.1 ± 14.4	10.6 ± 7.7
Medium Vein ($n=6$)	144.6 ± 51.7	38.6 ± 9.3	46.1 ± 6.3	7.4 ± 5.4	49.9 ± 16.9	59.6 ± 9.7	9.7 ± 10.4
Large Vein ($n=6$)	361.0 ± 116.9	36.9 ± 8.0	41.6 ± 9.5	4.8 ± 4.4	46.8 ± 14.4	54.0 ± 14.0	7.2 ± 6.7

N/A, not applicable.

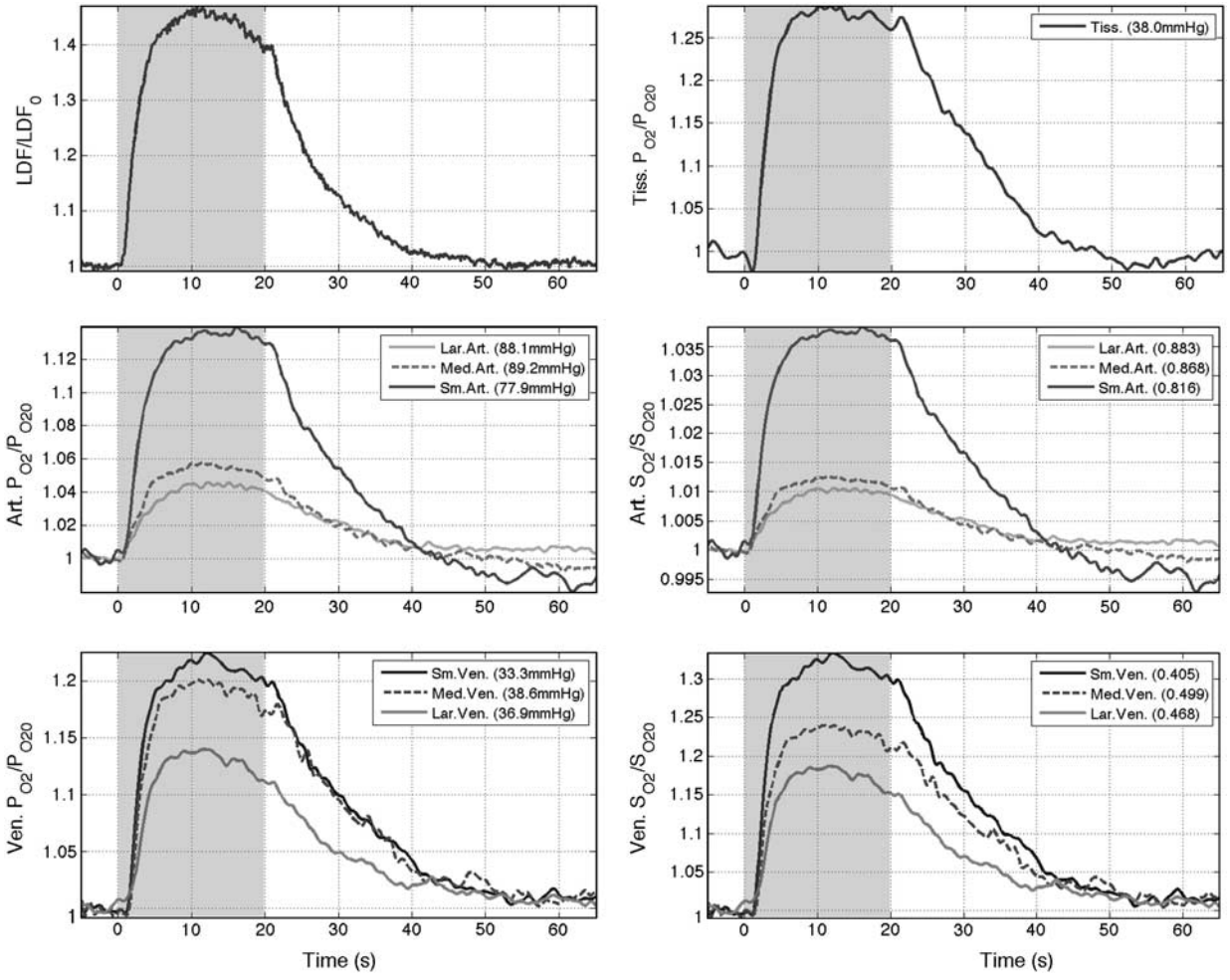

Figure 2 Average baseline-normalized CBF (top-left), arterial oxygen tension (middle-left), venous oxygen tension (bottom-left), tissue oxygen tension (top-right), and calculated arterial oxygen saturation (middle-right) and venous oxygen saturation (bottom-right) responses to somato-sensory stimulation in the seven locations sampled. The particular location and its corresponding resting P_{O2} and S_{O2} level are indicated in the figure legend. The stimulation period is indicated in gray in each panel.

in P_{O2} of 4.3%, 5.4%, 13.5%, 27.7%, 21.2%, 19.2% and 12.9% were observed in the sampled large artery, medium artery, small artery, tissue, small vein, medium vein and large vein locations, respectively. The data showed the largest changes in P_{O2} in the tissue, small vein and medium vein locations; however, all of the increases were determined to be significant based on *t*-tests with $P<0.05$. Among the sampled arterial locations, small arteries showed the largest increases in P_{O2} with stimulation. The P_{O2}

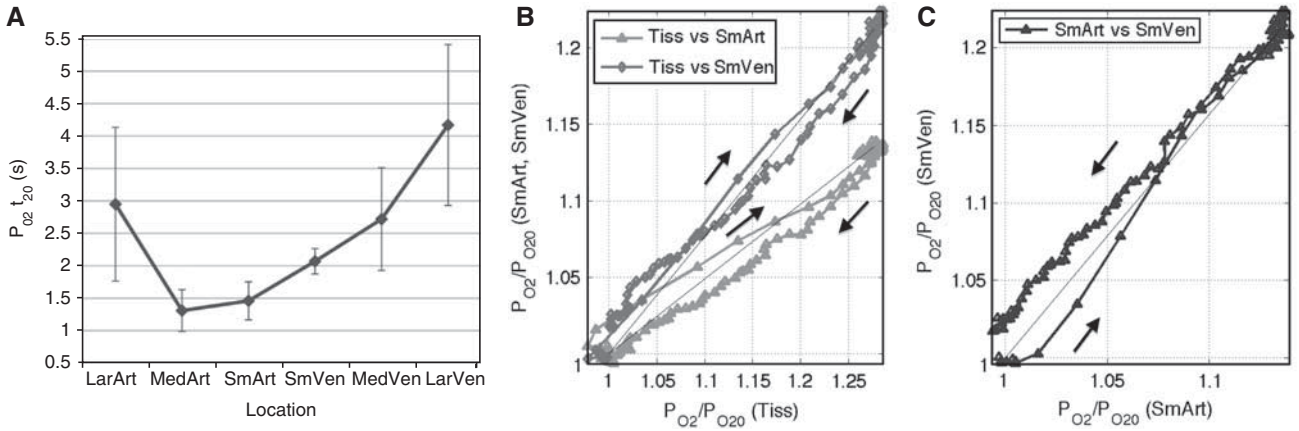

Figure 3 (**A**) The average t_{20} measured from the P_{O2} data is plotted as a function of the sampled location (see Supplementary Table S2; error bars denote the standard error). The average t_{20} measured from the LDF data was found to be 1.24 secs, suggesting that the P_{O2} increase with function follows from the blood flow response and propagates from the small vasculature to the larger vasculature. (**B**) Scatter plot of small artery and small vein against tissue oxygen tension (x-axis). This plot indicates that the changes in tissue P_{O2} lagged the changes in the small artery and small vein P_{O2} over 75% of the response onset. (**C**) Scatter plot of the small vein oxygen tension (y-axis) against the small artery oxygen tension (x-axis). It is evident from this plot that the increase in the small artery P_{O2} leads that of the small vein P_{O2} with stimulation onset. Direct proportionality lines have been included for each scatter pair (black line). Since the response offset is longer than the response onset, it contains a larger amount of point markers and can be used to differentiate these two phases of the response in each plot.

changes closely resembled the changes in CBF, although temporal delays were observed. A transient drop below baseline with stimulation onset was observed in the average tissue P_{O2} response with an amplitude of −2.1% that peaked 1.0 sec after stimulus onset. No detectable transient decreases below baseline were observed in the venous P_{O2} responses. Small post-stimulation undershoots were observed in the small artery and tissue location average time series. Since OIS and BOLD fMRI data are sensitive to the changes in blood oxygen saturation, these were also calculated from the P_{O2} data (see Figure 2). The largest difference between the measured P_{O2} time series and the calculated S_{O2} time series is the amplitude change (summarized in Table 1).

Temporally, the t_{20} of the P_{O2} time series was measured in all the animals tested (see Figure 3A and Supplementary Table S2). Although there was not a significant difference between the t_{20} values of the small and medium artery P_{O2}, these are both significantly earlier from the t_{20} of the small, medium and large vein P_{O2} (*t*-tests with $P<0.05$). The t_{20} values of the small and medium artery were also both earlier than the t_{20} of the large artery P_{O2} with $P<0.10$. The t_{20} values for the small, medium and large artery P_{O2} were not found to be significantly different from the LDF t_{20}. However, since the arterial P_{O2} changes are closely related to the changes in blood flow, the arterial t_{20} values suggest that, on average, the P_{O2} increase follows the CBF response originating from the small arterial vasculature and propagating upstream. These increases in P_{O2} also propagate into the venous vasculature, taking longer to reach the large vein. The scatter plot in Figures 3B and 3C illustrate the temporal differences between the small artery and small vein P_{O2} responses. The small artery P_{O2} leads the increase over the initial 50% of the response onset. It is worth noting that the changes in tissue (and venous) P_{O2} are slower than arterial P_{O2} partly due to the opposite effect of tissue oxygen metabolism on the P_{O2} level.

P_{o2} Gradient Along the Arterial-Venous Vasculature

The baseline and active P_{O2} values were collected for all subjects tested and plotted as a function of location in Figure 4. Under baseline conditions, the steepest gradients were observed on average between the sampled small artery and small vein (as expected), and also between the medium and small artery locations. The standard deviation of the oxygen tension measurements was not small but much of this variability is expected due to variability in caliber of the vessels sampled as well as variations in the physiological condition of the different animals tested (including the blood flow level). As a result, no significant differences were found between the different arterial locations, except between the arterial and venous locations (paired *t*-tests with $P<0.05$). Neural stimulation produced significant increases in P_{O2} in all of the sampled locations ($P<0.05$), although the change in the P_{O2} gradient was largest over the small artery, tissue and small vein locations. The corresponding S_{O2} was calculated and its gradient along the vasculature was observed to be on average shallower within the arteries. Evoked stimulation produced significant increases in the S_{O2} of all vein locations ($P<0.05$), but not in the arterial locations; the largest increase

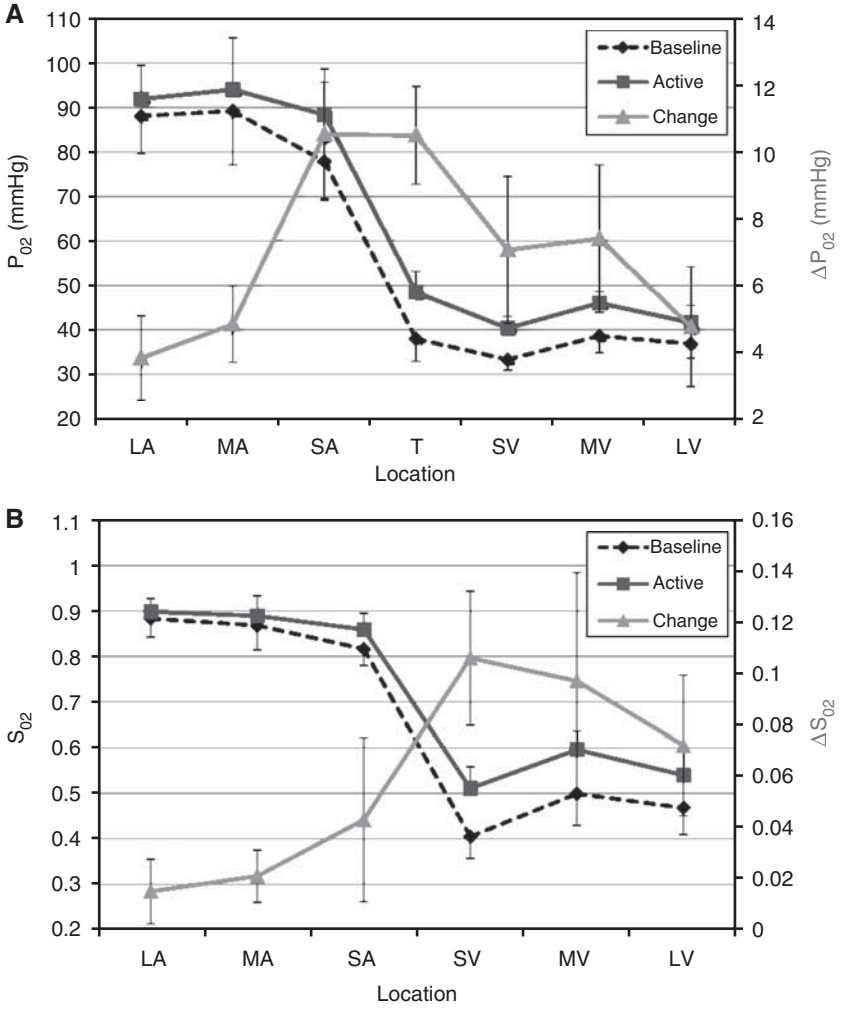

Figure 4 Average longitudinal oxygen tension (P_{O2}; **A**) and oxygen saturation (S_{O2}; **B**) gradient sampled by oxygen sensors positioned on a large surface artery (LA), medium-size surface artery (MA), small-size surface artery (SA; pre-penetrating), tissue (T; 300 μm depth), small-size surface vein (SV; post-emerging), medium-size surface vein (MV) and large surface vein (LV) on or adjacent to the somato-sensory area. The bars indicate the standard error. The average diameters of the vessels sampled are reported in Table 1. The two curves represent the average longitudinal gradient during the rest period (5 secs preceding stimulation; black line) and activated period (between 10 and 20 secs after stimulation onset; blue line). The absolute differences in P_{O2} and S_{O2} induced by forepaw stimulation are also plotted (red line). The systemic arterial oxygen tension and saturation were 133.3 mm Hg and 96.9%, respectively, measured at the femoral artery.

in S_{O2} was observed in the small vein locations. The increase in the S_{O2} gradient was significant between the sampled arterial and venous locations, but not within the arterial or venous locations sampled.

Stimulation-induced OIS Responses

The ROI-averaged data recorded by OIS (620 nm) showed some differences in its temporal evolution compared to the P_{O2} measurements. The large artery ROI showed a small but sustained decrease in signal that lasted over the stimulation period (see Figure 5B, top-left panel). The magnitude of the decrease initially peaked at 1.8 secs following stimulation onset (−0.20%). This observation was evident in the difference image in large arteries and, occasionally, also in medium and small arteries (a sample image is presented in Figure 5A; although the stimulation parameters were different in this image, the overall features were the same). The medium and small artery ROIs also showed similar transient decreases in signal of −0.18% and −0.21%, respectively, that peaked at 1.4 and 1.7 secs after stimulation onset, respectively. The signal in these ROIs, however, increased over pre-stimulation baseline levels after 2.7 secs (Figure 5B, top-left panel). Both tissue ROIs, one centered over the penetration point of the tissue P_{O2} probe and another over the centroid of activation, also showed bi-phasic responses with stimulation onset (Figure 5B, bottom-left panel) which showed minimum peak decreases of −0.13% and −0.14%, respectively, occurring 1.3 secs after stimulation onset, and also positive peak increases of

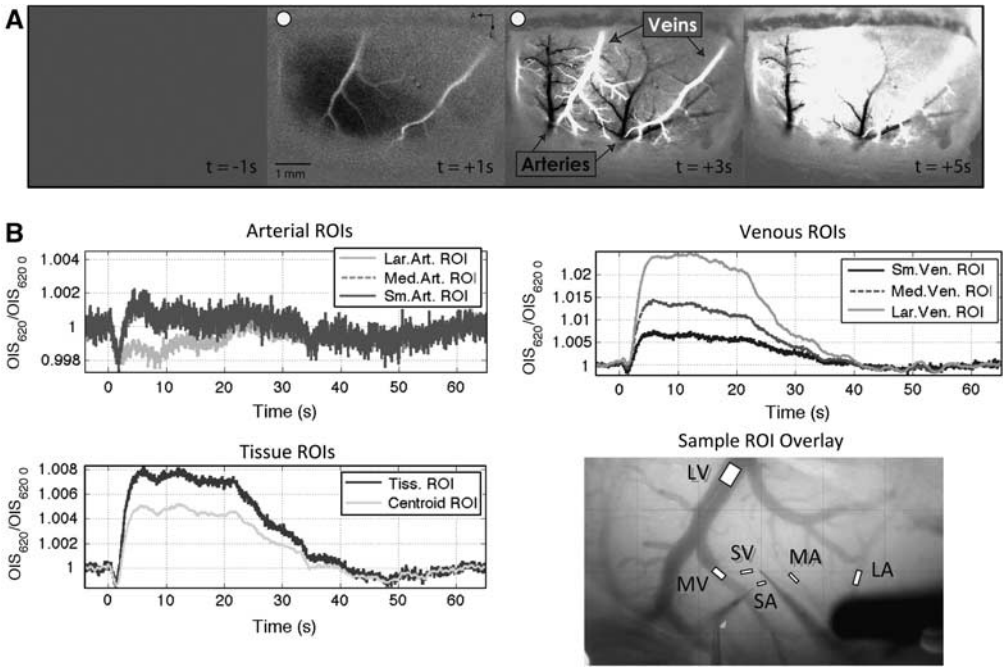

Figure 5 (**A**) Sample optical imaging sequence of a preliminary mapping experiment in one subject (see Materials and Methods section for experimental detail). Each image frame represents the average of 1 sec around the time indicated in each image. The stimulus was delivered between t = 0 and t = 4 secs, and these images have been marked with a red dot to indicate they are stimulation images. The dark and bright vessels in the t = + 3 frame correspond to the arteries and veins, respectively. An extended sequence has been included in Figure S2 in the Supplementary Material. (**B**) Average OIS time series obtained from 8 ROIs: (top-left panel) Large artery, medium artery and small artery ROIs; (bottom-left panel) tissue ROI centered around the tissue P_{O2} probe and tissue ROI centered on the centroid of activity as determined from an OIS pre-mapping experiment; (top-right panel) small vein, medium vein and large vein ROIs. These panels show the optical signal response to somato-sensory stimulation at those locations normalized relative to baseline. The stimulation period is indicated in gray in each panel. A sample of the location of the vessel ROIs is illustrated in the bottom-right panel.

+0.76% and +0.50% for each tissue ROI, respectively. After stimulation offset, small decreases below baseline also observed in both tissue ROIs. In the veins, the average magnitude of the early dip was observed to decrease as the venous vessel location increased (from −0.13% to −0.08% and 0% in the small, medium and large vein ROIs, respectively; see Figure 5B; top-right panel); however, its temporal location was about the same over all of the venous ROIs (~1.3 secs after stimulation onset). The OIS signal plateau increased with increasing venous vessel size (from 0.69% to 1.37% and 2.44% in small, medium and large vein ROIs, respectively). The post-stimulation undershoot was also observed in all the venous ROIs and its amplitude decreased as the venous vessel size increased.

The t_{50-dip} and t_{20} were also measured for the OIS data, (see Supplementary Table S2 in the Supplementary Material). The OIS dip has been hypothesized to be indicative of metabolic processes (Vanzetta *et al*, 2005), although it may also represent increases in blood volume. On average, the t_{50-dip} propagates from the tissue ROI to the small, medium and large vein ROIs. Interestingly, the OIS t_{50-dip} measured from the tissue probe OIS ROI (0.64 ± 0.35 secs) is similar to the t_{50-dip} measured from the tissue P_{O2} time series (0.53 ± 0.31 secs; $n = 9$). All of the artery t_{50-dip} values were found to be larger than those in the veins, on average; only the large artery t_{50-dip} was significantly different to all the venous t_{50-dip} with $P < 0.05$. While the OIS dip in the venous ROIs may be representative of increases in metabolism, the dip in the arteries is likely due to increases in blood volume (and blood flow). In fact, there was sufficient contrast in the OIS images to track the diameter of the targeted medium and large arteries and veins (Supplementary Figure S1). Detectable average increases of 4% and 6% were evident in the large and medium arterial diameter, respectively, while none were detected in the large and medium venous diameter (see Figure 6).

Discussion

The principal objective of this work was to measure the changes in arterial, tissue and venous P_{O2} that take place with neural stimulation. Stimulation of the rat forepaw induced measurable increases in P_{O2} throughout the vasculature. To our knowledge, this is the first report of direct measurements of the cerebrovascular P_{O2} with brain function. Of particular interest is that the largest fractional increases in

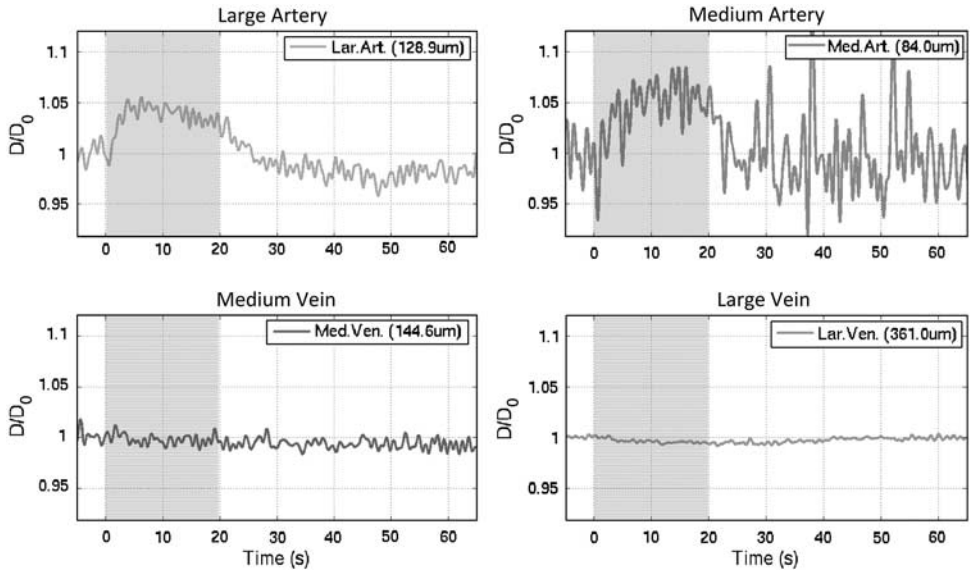

Figure 6 Estimated average changes in the large artery (top-left panel), medium artery (top-right), medium vein (bottom-left) and large vein (bottom-right) vessel diameter calculated from the OIS data (620 nm; $n = 4$). The image contrast was not sufficient to calculate the vessel diameter in the small artery and small vein locations in all the subjects tested, and in the large and medium artery locations in four of the subjects tested. In fact, the large amount of noise in the medium artery location reflects the decrease in the image contrast at this location.

vascular P_{O2} were measured in the small vein and the small artery. Changes in S_{O2} showed the largest increases in small veins while the increase in small arteries was small. Temporally, the increases in the vascular P_{O2} were first observed in the small/medium artery followed by the small vein. Not surprisingly, the most latent increase in P_{O2} was observed in the large vein. The ensuing discussion shows the following: (1) These findings are in agreement with the notion that BOLD fMRI is largely sensitive to the changes in venous oxygenation, and (2) the increases in arterial oxygen tension are significant, contribute to the hyper-oxygenation of tissue and, mostly likely, also to the BOLD fMRI signal.

The P_{O2} measurements of the large artery location corresponded to the largest middle cerebral artery branch feeding the forepaw area. Similarly, the P_{O2} measurements of the large vein location corresponded to the largest vein draining blood from the forepaw area, typically the middle cerebral vein. The baseline P_{O2} gradient measured between these two physiological end-points showed a noticeable steepening of the P_{O2} gradient from the medium artery location to the small vein location. Similar findings were reported by Vovenko for his measurements of the baseline P_{O2} in cerebral vessels (Vovenko, 1999). A comparison of the absolute P_{O2} values show larger baseline values for this work probably due to the supplementary amount of oxygen added to the breathing mixture ($\sim$10% O_2). Nonetheless, our results are in good agreement with the average oxygen gradient measured by Vovenko relative to the largest artery measured. In this work, a relatively large amount of variability in the P_{O2} measurements was observed (and expected) across animals. This variability is due to the different vessel sizes targeted and to differences in the physiological condition of the animals during the experiment. Notwithstanding, the results obtained in each subject tested and the targeted blood vessels were very consistent and reproducible. The vascular P_{O2} measurements were sampled from the surface of the vessel, not the intraluminal space, and the vessel wall thickness is known to vary with vessel diameter (i.e. ratios of 25% and 10% and are commonly accepted for arteries and veins, respectively) (Burton, 1954). Hence, the real average intra-luminal P_{O2} is likely to be higher, especially in arteries because of their thicker vessel wall. The P_{O2} gradient in the radial direction around the vessel wall has been measured to be as high as 1.2 mm Hg/μm (Sharan, *et al*, 2008). This source of variability was minimized by the selection criteria of the tip diameter of the vascular P_{O2} probe (4 μm) to ensure its sensitivity of the intraluminal space. While the vessel wall thickness of the veins is smaller, the venous P_{O2} gradient was also somewhat noisy. This was observed during the experiment and repositioning the probe up or down the same vessel was not observed to change the measured P_{O2} level much. Vovenko also reported some variability in the venous P_{O2} gradient. It is possible that this could be due to variations in the P_{O2} within the veins, especially near branching points. In several experiments, the position of the probes was not ideal, mostly because the centroid of the forepaw area in the somato-sensory cortex was frequently near the large artery and/or the large veins (these were excluded from the centroid calculation; for example, see darkening in Figure 5A). However, the final placement of the small artery, small vein

and tissue P_{O2} probes was always verified to be well within the forepaw area based on the preliminary optical imaging map.

Evoked brain stimulation was observed to increase the P_{O2} throughout the targeted vasculature, indicating a large span for the changes in CBF, including the large artery (a prominent branch of the middle cerebral artery). Another interesting finding was that the average increase in the small artery P_{O2} was very close to that obtained in tissue. This indicates a dominant role for this size/type arterial vessel in blood flow regulation since the change in arterial P_{O2} is dominated by changes in CBF. A recent report from our group concluded that increases in the capillary P_{O2} supplied by increases in the upstream arterial oxygenation were necessary to explain the observed functional increases in tissue P_{O2} (Vazquez *et al*, 2008). The results obtained in this work are in good agreement with those findings. The largest increase in S_{O2} was calculated to take place in small surface veins with progressively smaller changes in the larger venous vasculature, most likely due to the dilution of the oxygenation changes draining from non-activated cortical areas. In general, the results obtained are in agreement with optical imaging results in the literature that show increases in Hbt and HbO_2 in pre-penetrating arterial branches (Berwick *et al*, 2005; Hillman *et al*, 2007). The quantification of the absolute P_{O2} changes at the sampled vascular and tissue locations have provided substance to these findings in light of the non-linear relationship between S_{O2} and P_{O2}. Temporally, the results obtained suggest that the blood flow-driven increases in P_{O2} start at small and medium arteries and propagate to the venous and larger arterial vasculature within 1.5 secs. These temporal changes are in agreement with optical imaging studies in the literature (Vanzetta *et al*, 2005; Berwick *et al*, 2005; Hillman *et al*, 2007; Iadecola *et al*, 1997) where arterial and venous signals were extracted to investigate the temporal propagation of the vascular response. In those studies the vascular response originated in arterioles and spread to capillaries and venules; in addition, the magnitude of arterial response was smaller in larger caliber arterial vessels. Both of these trends are also evident in our results. Also in line with those studies was the observation that the metabolic response onset (represented by t_{50-dip}) preceded the blood flow response.

Optical imaging of intrinsic signal was also acquired in this study to generalize our findings to the larger vascular network supplying oxygen to the somato-sensory cortex. The temporal changes averaged over ROIs placed near the P_{O2} recording sites show two distinct features. First, the arterial OIS changes are of opposite polarity to the arterial P_{O2} changes. Second, while the magnitude of the venous P_{O2} increase was observed to decrease in larger veins, the average venous OIS signal was observed to increase in larger veins. These features are evident in the OIS difference images in Figure 5A. These two features can be explained as follows. The absorption of 620 nm light is dominated by deoxy-hemoglobin content and, therefore, decreases in OIS signal imply increases in deoxy-hemoglobin. In this fashion, although the arterial P_{O2} was observed to increase, a larger increase in arterial volume would reflect a decrease in OIS signal. The vessel diameter near the large and medium arterial locations was found to increase (Figure 6), indicating that the decreases in arterial OIS signal are the result of dominant increases in the arterial blood volume. In addition to optical imaging, there is a growing literature demonstrating significant arterial blood volume increases using MRI (Lee *et al*, 2001; Kim *et al*, 2007). The larger increase in the OIS signal of large veins is likely due to the increase in S_{O2} in these vessels and also to the larger volume of the veins. Notwithstanding, the OIS difference images in Figure 5A show that the changes observed in arteries and veins are fairly homogenous and that the P_{O2} findings can be generalizable across arteries and veins supplying the somato-sensory cortex.

Similar to the P_{O2} data, the temporal evolution of the OIS dip in the arterial ROIs shows a slight average progression of the blood volume (and blood flow) response that also originates in the smaller arterial vasculature ($t_{50-dip} = 0.64$ secs) and propagates to the larger arterial vasculature ($t_{50-dip} = 0.80$ secs; see Supplementary Table S2). However, the dip response observed in the venous OIS data was not evident in the venous P_{O2} data. It is possible that this discrepancy is due to a lack in sensitivity since small P_{O2} dips were present in the small vein location of two subjects and the medium vein location of one subject (the larger diameter of the tissue P_{O2} probe provides better sensitivity compared to the smaller probes used to measure the vascular P_{O2}). Considering dip measurements (t_{50-dip}) from these P_{O2} data subsets, the overall observation of the dip propagating from tissue to the larger venous vasculature is maintained.

The results obtained here have several implications for the quantification of BOLD fMRI signals; most notably, the measured baseline arterial P_{O2} in the small arterial location shows that the intra-cortical arterial oxygen saturation in rodents is less than the assumed 100%, indicating that intra-cortical arteries likely contribute to the BOLD signal. The extent of this contribution based solely on our P_{O2} measurements is confounded by P_{O2} contributions from the vessel wall which would underestimate the intra-luminal arterial P_{O2} and S_{O2}. Nonetheless, if the intra-cortical arterial oxygen saturation is less than 100%, then the increases in arterial P_{O2} and arterial blood volume may also be significant enough to impact the BOLD signal change. While it is possible that the net arterial oxygenation (deoxy-hemoglobin) may be negligible since the increases in P_{O2} may balance the increases in blood volume, a blood oxygenation effect was consistently observed in the OIS data. Therefore, the calculation of CMR_{O2} from

BOLD fMRI data may require accounting for the baseline arterial oxygen saturation, increases in the arterial oxygen saturation and increases in the arterial blood volume (usually assumed to not contribute to the overall BOLD signal; not to mention, negligible increases in venous volume). Current models are still suitable to quantify the average CMR_{O2} change over large ROIs where the input arterial oxygenation is closer to the systemic arterial S_{O2} and the increases in arterial S_{O2} are very small. However, these assumptions appear to break down over smaller intra-cortical brain regions estimated to be on order of 1 mm. An in-depth investigation of the impact of these results on the quantification of oxygen metabolism from hemoglobin-sensitive data (e.g. fMRI and OIS) is currently under way. It is worth mentioning that the oxygen saturation results reported in this work (see Table 1) are for rodent hemoglobin; the oxygen saturation of human hemoglobin will be higher assuming the same P_{O2} values. For example, the S_{O2} of the large and small arterial locations would be 95.6% (vs 88.3% in Table 1) and 89.2% (vs 81.6%) using a P50 of 26 mm Hg for human hemoglobin. Therefore, care muse be taken if these results are extrapolated to human studies. It is also worth mentioning that one fundamental difference between the OIS signal changes measured in this work and that of BOLD fMRI is that deoxy-hemoglobin-sensitive OIS (intravascular light absorbance) corresponds closely with the extra-vascular BOLD fMRI signal. That is, the change in the amount of hemoglobin in a blood vessel is proportional to the amount of light absorbed by that vessel in OIS (e.g. 620 nm) and also to the change in the extra-vascular BOLD signal. On the other hand, the intra-vascular BOLD fMRI signal will depend on the blood oxygen saturation, not the amount, since the magnetic field differences experienced by intra-vascular water depend on the deoxyhemoglobin concentration.

Acknowledgements

Sources of funding: This work was supported by NIH grants F32-NS056682 and RO1-EB003375.

Conflict of interest

The authors declare no conflict of interest.

References

Ances BM, Buerk DG, Greenberg JH, Detre JA (2001) Temporal dynamics of the partial pressure of brain tissue oxygen during functional forepaw stimulation in rats. *Neurosci Lett* 306:106–10

Berwick J, Johnston D, Jones M, Martindale J, Redgrave P, McLoughlin N *et al.* (2005) Neurovascular coupling investigated with two-dimensional optical imaging spectroscopy in rat whisker barrel cortex. *Eur J Neurosci* 22:1655–66

Burton AC (1954) Relation of structure to function of the tissues of the wall of blood vessels. *Physiol Rev* 34:619–42

Boas DA, Strangman G, Culver JP, Hoge RD, Jasdzewski G, Poldrack RA *et al.* (2003) Can the cerebral metabolic rate of oxygen be estimated with near-infrared spectroscopy? *Phys Med Biol* 48:2405–18

Boas DA, Gaudette T, Strangman G, Cheng X, Marota JJ, Mandeville JB (2001) The accuracy of near infrared spectroscopy and imaging during focal changes in cerebral hemodynamics. *Neuroimage* 13:76–90

Davis TL, Kwong KK, Weisskoff RM, Rosen BR (1998) Calibrated functional MRI: mapping the dynamics of oxidative metabolism. *Proc Natl Acad Sci USA* 95:1834–9

Fatt I (1976) *The polarographic oxygen sensor: Its theory of operation and its application in biology, medicine, and technology*. CRC Press

Fukuda M, Wang P, Moon CH, Tanifuji M, Kim SG (2006) Spatial specificity of the enhanced dip inherently induced by prolonged oxygen consumption in cat visual cortex: implication for columnar resolution functional MRI. *Neuroimage* 30:70–87

Gray LH, Steadman JM. (1964) Determination of the oxyhaemoglobin dissociation curves for mouse and rat blood. *J Physiol* 175:161–71

Gibson QH, Kreuzer F, Meda E, Roughton FJ (1955) The kinetics of human haemoglobin in solution and in the red cell at 37 degrees C. *J Physiol* 129:65–89

Hall RD, Lindholm EP (1974) Organization of motor and somatosensory neocortex in the albino rat. *Brain Res* 66:23–8

Hillman EM, Devor A, Bouchard MB, Dunn AK, Krauss GW, Skoch J *et al.* (2007) Depth-resolved optical imaging and microscopy of vascular compartment dynamics during somatosensory stimulation. *Neuroimage* 35:89–104

Horecker BL (1943) The absorption spectra of hemoglobin and its derivatives in the visible and near infra-red regions. *J Biol Chem* 148:173–83

Iadecola C, Yang G, Ebner TJ, Chen G (1997) Local and propagated vascular responses evoked by focal synaptic activity in cerebellar cortex. *J Neurophysiol* 78:651–9

Kim SG (1995) Quantification of relative cerebral blood flow change by flow-sensitive alternating inversion recovery (FAIR) technique: application to functional mapping. *Magn Reson Med* 34:293–301

Kim SG, Rostrup E, Larsson HB, Ogawa S, Paulson OB (1999) Determination of relative CMRO2 from CBF and BOLD changes: significant increase of oxygen consumption rate during visual stimulation. *Magn Reson Med* 41:1152–61

Kim T, Hendrich KS, Masamoto K, Kim SG (2007) Arterial versus total blood volume changes during neural activity-induced cerebral blood flow change: implication for BOLD fMRI. *J Cereb Blood Flow Metab* 27:1235–1247

Kwong KK, Belliveau JW, Chesler DA, Goldberg IE, Weisskoff RM, Poncelet BP *et al.* (1992) Dynamic magnetic resonance imaging of human brain activity during primary sensory stimulation. *Proc Natl Acad Sci USA* 89:5675–9

Lee SP, Duong TQ, Yang G, Iadecola C, Kim SG (2001) Relative changes of cerebral arterial and venous blood volumes during increased cerebral blood flow: implications for BOLD fMRI. *Magn Reson Med* 45:791–800

Masamoto K, Omura T, Takizawa N, Kobayashi H, Katura T, Maki A *et al* (2003) Biphasic changes in tissue partial pressure of oxygen closely related to localized neural activity in guinea pig auditory cortex. *J Cereb Blood Flow Metab* 23:1075–84

Masamoto K, Vazquez A, Wang P, Kim SG (2008) Trial-by-trial relationship between neural activity, oxygen consumption, and blood flow responses. *Neuroimage* 40:442–50

Mayhew J, Johnston D, Berwick J, Jones M, Coffey P, Zheng Y (2000) Spectroscopic analysis of neural activity in brain: increased oxygen consumption following activation of barrel cortex. *Neuroimage* 12:664–75

Popel AS (1989) Theory of oxygen transport to tissue. *Crit Rev Biomed Eng* 17:257–321

Severinghaus JW (1993) History and recent developments in pulse oximetry. *Scand J Clin Lab Invest Suppl* 214:105–11

Sharan M, Vovenko EP, Vadapalli A, Popel AS, Pittman RN (2008) Experimental and theoretical studies of oxygen gradients in rat pial microvessels. *J Cereb Blood Flow Metab* 28:1597–604

Shulman RG, Hyder F, Rothman DL (2001) Lactate efflux and the neuroenergetic basis of brain function. *NMR Biomed* 14:389–96

Thompson JK, Peterson MR, Freeman RD. (2003) Single-neuron activity and tissue oxygenation in the cerebral cortex. *Science* 299:1070–2

Tsai AG, Johnson PC, Intaglietta M (2003) Oxygen gradients in the microcirculation. *Physiol Rev* 83:933–63

Vanzetta I, Hildesheim R, Grinvald A (2005) Compartment-resolved imaging of activity-dependent dynamics of cortical blood volume and oximetry. *J Neurosci* 25:2233–44

Vazquez AL, Masamoto K, Kim SG (2008) Dynamics of oxygen delivery and consumption during evoked neural stimulation using a compartment model and CBF and tissue P(O2) measurements. *Neuroimage* 42:49–59

Vovenko E (1999) Distribution of oxygen tension on the surface of arterioles, capillaries and venules of brain cortex and in tissue in normoxia: an experimental study on rats. *Pflugers Arch* 437:617–23

Weiss HR, Buchweitz E, Sinha AK (1983) Effect of hypoxic-hypocapnia on cerebral regional oxygen consumption and supply. *Microvasc Res* 25:194–204

Supplementary Information accompanies the paper on the Journal of Cerebral Blood Flow & Metabolism website (http://www.nature.com/jcbfm)